



1 **Inferring the Photolysis Rate of NO₂ in the Stratosphere**

2 **Based on Satellite Observations**

3 Jian Guan¹, Susan Solomon¹, Sasha Madronich^{2,3}, Douglas Kinnison²

4 ¹Department of Earth, Atmospheric, and Planetary Sciences, MIT; Cambridge, MA, 02139, USA

5 ²Atmospheric Chemistry Observations and Modeling Laboratory, National Center for Atmospheric Research, Boulder,
6 CO, 80301, USA

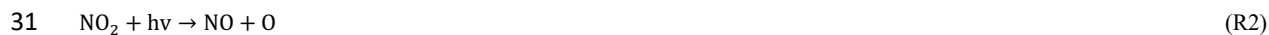
7 ³USDA UV-B Monitoring and Research Program, Natural Resource Ecology Laboratory Colorado State University, Fort
8 Collins, Colorado, 80523, USA

9 Correspondence to: Jian Guan (jianguan@mit.edu)

10 **Abstract.** NO and NO₂ (NO_x) play major roles in both tropospheric and stratospheric chemistry. This paper provides a novel
11 method to obtain a global and accurate photodissociation coefficient for NO₂ based on satellite data. The photodissociation
12 coefficient J_{NO₂} dominates the daytime diurnal variation of NO_x photochemistry. Here the spatial variation of J_{NO₂} in 50° S-90° S
13 in December from 20-40 km is obtained using data from the Michelson Interferometer for Passive Atmospheric Sounding (MIPAS)
14 experiment. Because NO and NO₂ exchange rapidly with one another in the daytime, the J_{NO₂} can be attained assuming steady
15 state, and the results are shown to be consistent with model results. The J_{NO₂} value decreases as the solar zenith angle increases
16 and has a weak altitude dependence. A key finding is that the satellite-derived J_{NO₂} increases in the polar regions in good agreement
17 with model predictions, due to the effects of ice and snow on surface albedo. Thus, the method presented here provides an
18 observations-based check on the role of albedo in driving polar photochemistry.

19 **1 Introduction**

20 Fast photochemistry in the Earth's atmosphere is driven by sunlight and affects the diurnal variation of many species. The properties
21 of sunlight entering the stratosphere, including light intensity and its energy distribution, depend on the solar zenith angle, as well
22 as the overhead concentrations of oxygen and ozone and the reflective properties of the underlying troposphere. Further, the solar
23 zenith angle is related to latitude, season, and local time. The sunlight entering the stratosphere determines the photochemical rates
24 in the stratosphere, thus affecting stratospheric chemistry, and the diurnal variations of species concentration is one of the impacts.
25 Therefore, diurnal variation observations provide key information in analyzing the photochemical properties of the stratosphere.
26 NO_x chemistry is one of the most important elements of stratospheric chemistry and plays a leading role in controlling stratospheric
27 ozone concentration (Crutzen, 1979; Johnston, 1971; Crutzen, 1970). The photodissociation coefficient J_{NO₂} quantifies the process
28 of NO₂ photolysis into NO, thus affecting the diurnal variation of NO_x. The stratospheric NO and NO₂ abundances are controlled
29 by the following reactions:



34 Because of the short lifetime of NO and NO₂, they are in steady state within the sunlit stratosphere. Therefore, the following
35 equation holds:



$$36 \quad \frac{[\text{NO}]}{[\text{NO}_2]} \approx \frac{J_{\text{NO}_2} + k_{\text{O}+\text{NO}_2} \times [\text{O}]}{(k_{\text{NO}+\text{O}_3} \times [\text{O}_3] + k_{\text{NO}+\text{ClO}} \times [\text{ClO}])} \quad (1)$$

37 A number of studies on the diurnal variation of NOx and J_{NO₂} in the stratosphere have been reported, based on models or airborne
38 observations. Fabian et al. (1982) used a two-dimensional model to examine the diurnal variations of NOx at different altitudes.
39 Many studies of the NOx diurnal variation based on airborne observations which were then compared with models (Pommereau,
40 1982; Roscoe et al., 1986; Kawa et al., 1990). Madronich et al. (1985) measured J_{NO₂} in the stratosphere utilizing a balloon platform
41 and compared it to a model; they showed that the J_{NO₂} value has a weak altitude dependence. Webster and May (1987) measured
42 the diurnal variation of NOx and J_{NO₂} simultaneously utilizing a balloon. Del Negro et al. (1999) calculated J_{NO₂} based on the
43 concentrations of NO, NO₂, O₃, ClO, and HO₂ measured on an aircraft and BrO from a model, and compared them with a model.
44 They found that the J_{NO₂} inferred from the data assuming steady state matched their model well. Moreover, it has been emphasized
45 that albedo has a substantial effect on J_{NO₂} (Madronich, 1987; Bösch et al., 2001; Laepple, 2005; Walker et al., 2022). Further, the
46 surface albedo over ice and snow has a large and important effect on tropospheric chemistry in the polar regions (Walker et al.,
47 2022) due in large part to its effect on J_{NO₂}, highlighting the need to evaluate J_{NO₂} on a large scale. Surface radiometers have also
48 been used to infer information about J_{NO₂} for different sky conditions in the troposphere (Shetter et al., 1992; Junkermann et al.,
49 1989). However, aircraft, surface radiometers, or balloon measurements are all local and the amount of data is therefore limited.
50 At the same time, models are based on theoretical calculations and require measured data for verification. These considerations
51 are the motivation for this paper, in which satellite data are used to characterize J_{NO₂} on a global basis, with particular emphasis on
52 values obtained over ice and snow.

53 Satellite measurements of NOx allow elucidation of its zenith angle and albedo dependence. The global concentrations of NO,
54 NO₂, and related species as discussed below can be easily obtained using satellite data and used to determine J_{NO₂} at different
55 latitudes, albedo, and altitudes. Solomon et al. (1986) reported satellite observations of the NO₂ diurnal variation in the stratosphere
56 at solar zenith angles ranging from about 35 to 110 degrees but concurrent NO data were not available. Anderson et al. (1981)
57 employed a similar method to study the zenith angle variation of mesospheric O₃. The Michelson Interferometer for Passive
58 Atmospheric Sounding (MIPAS) is a backscatter Fourier transform spectrometer carried on Envisat, measuring not only NO₂ but
59 also NO and O₃, as well as ClO, all of which are used here in inferring J_{NO₂} (see below). MIPAS was designed and operated for
60 the measurement of atmospheric species from space and can detect limb emission in the middle atmosphere with high spectral
61 resolution and low-noise performance (Fischer et al., 2008).

62 In this work, the novel method of obtaining the zenith angle dependence of NOx and J_{NO₂} using satellite data in summer over the
63 polar cap is reported, taking 50° S-90° S in December in 20-40 km as an example. The diurnal variations of NOx and J_{NO₂} at
64 different altitudes are described. J_{NO₂} changes with latitude are discussed and a J_{NO₂} map in the Antarctic is used to elucidate
65 albedo effects. In summary, this work shows a method for obtaining NOx diurnal variation and accurate J_{NO₂} based on satellite
66 data, expanding the way to attain information on this key photodissociation coefficient.

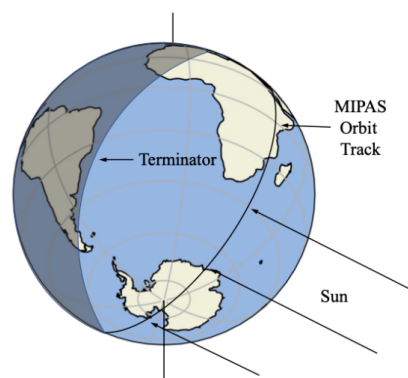
67 2 Data and Methods

68 2.1 MIPAS Data

69 The vertical resolution of MIPAS is approximately 3 km and the horizontal resolution of MIPAS is 30 km, and the vertical scan
70 range is 5-150 km. Satellite operation was stopped temporarily in March 2004 due to technical issues and resumed in January 2005
71 in a new operation mode. MIPAS allows near complete global coverage, ranging from 87° S to 89° N obtained about every three



72 days by 73 scans per orbit and 14.3 orbits per day. Each day the satellite passes through the same latitude at two local times
73 (ascending side and descending side, as shown in Fig. 1). Therefore, for this dataset, there are only two solar zenith angles at each
74 latitude. We therefore focus on 50° S-90° S in the polar day, in December 2009, where there are as many solar zenith angles as
75 possible in a relatively small latitude range. In this paper, the NO, NO₂, O₃, ClO, temperature and pressure data were from V8 level
76 2 MIPAS retrievals (Kiefer et al., 2021, 2022). The reported precision between 20 km and 40 km is 5-15 % for NO (Funke et al.,
77 2022; Sheese et al., 2016), 5-15 % for NO₂ (Wetzel et al., 2007), 2-3 % for O₃ (Laeng et al., 2015) and more than 35 % for ClO
78 (Von Clarmann et al., 2009).



79

80 Figure 1. Schematic representation of the MIPAS orbit at high latitude in December showing the ascending (dayside) and
81 descending (nightside) portions of the orbit and the terminator.

82 2.2 Model Calculations

83 The Whole Atmosphere Community Climate Model version 6 (WACCM6) is used in this study. WACCM6 is a component of the
84 Community Earth System Model version 2 (CESM2; Gettelman et al., 2019; Danabasoglu et al., 2020). The horizontal resolution
85 is 1.9° latitude × 2.5° longitude and the with 88 vertical levels up to about 140 km, with the altitude resolution increasing from 0.1
86 km near the surface to 1.0 km in the upper troposphere–lower stratosphere (UTLS) and 1–2 km in the stratosphere. This work uses
87 the specified dynamics version of WACCM6, where the atmosphere below 50 km is nudged to the Modern-Era Retrospective
88 Analysis for Research and Applications, version 2 (MERRA-2; Gelaro et al., 2017), temperature and wind fields with a relaxation
89 time of 50 h. The chemistry mechanism includes a detailed representation of the middle atmosphere, with a sophisticated suite of
90 gas-phase and heterogeneous chemistry reactions, including the Ox, NO_x, HO_x, ClO_x, and BrO_x reaction families. There are ~100
91 chemical species and ~300 chemical reactions. Reaction rates are updated following Jet Propulsion Laboratory (JPL) 2015
92 recommendations (Burkholder et al., 2015). The photolytic approach is based on both inline chemical modules (<200nm) and a
93 lookup table approach (>200-750nm; see Kinnison et al., 2007). The look-up table (LUT) approach uses the Tropospheric
94 Ultraviolet-Visible Radiation Model (TUV4.2; Madronich, 1987; Madronich and Weller, 1990), an advanced radiation transfer
95 model widely used by the scientific community, using the four-stream pseudospherical discrete ordinates option. Model values for
96 December 2009 at the same times and location as the satellite data are selected to compare with the satellite data, and denoted
97 “Model”.

98 2.3 Chemical Equation

99 NO is assumed to be in a steady state in the sunlit atmosphere at 20–40 km at least for a zenith angles less than 94°, due to its short
100 lifetime. Using the chemistry discussed above, J_{NO_2} can then be expressed as



101
$$J_{NO_2} = \frac{[NO]}{[NO_2]} \times (k_{NO+O_3} \times [O_3] + k_{NO+ClO} \times [ClO]) - k_{O+NO_2} \times [O] \quad (2)$$

102 Where k is the rate constant, J_{NO_2} is the photodissociation coefficient of NO_2 , and $[O_3]$ is the concentration of O_3 .

103 To obtain the concentration of O , O is assumed to be in a steady state with ozone at 20-40 km. The concentration of O can be
 104 expressed as

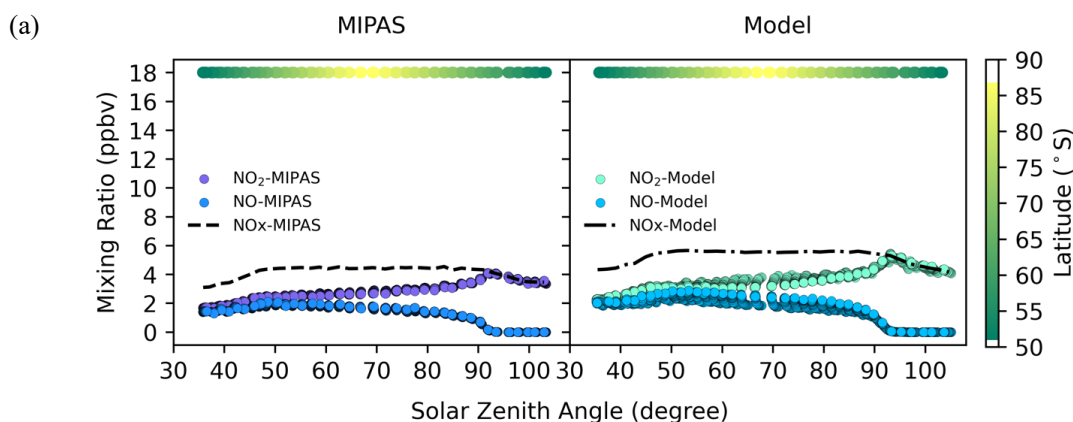
105
$$[O] = \frac{J_{O_3} \times [O_3]}{k_{O+O_2} + M \times [O_2] \times [M]} \quad (3)$$

106 It is worth noting that J_{O_3} in the Eq. (3) comes from the model here, which is a limitation of this study. However, in the stratosphere
 107 below about 33 km $[O]$ has a small effect on J_{NO_2} (less than 8.1 percent). ClO can similarly be ignored when altitudes are less than
 108 35 km, where ClO concentrations are small; otherwise using ClO data from MIPAS would introduce large and unnecessary
 109 uncertainty. HO_2 and BrO both can react with NO but they are not measured by MIPAS and their contributions to the partitioning
 110 between NO and NO_2 are negligibly small at the altitudes considered here. Therefore, we don't consider them in this paper.

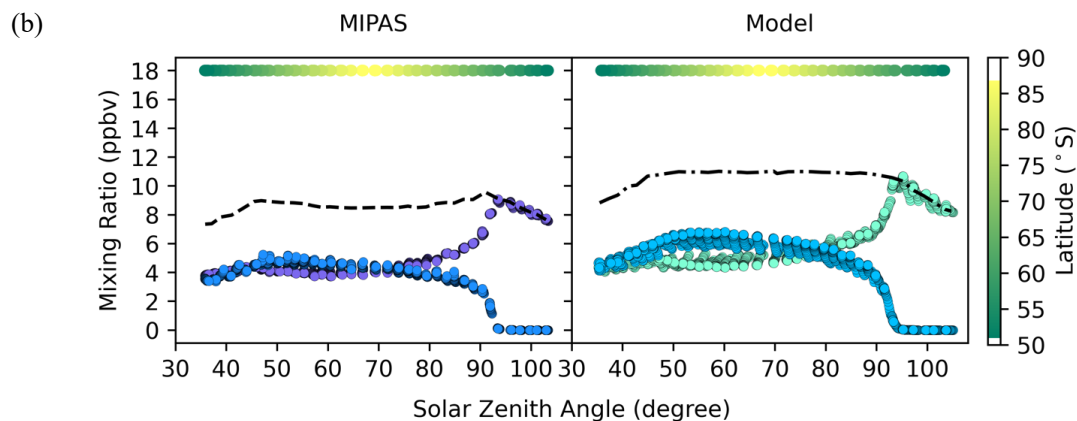
111 **3 Results and Discussion**

112 **3.1 NO_x Concentration at different altitudes**

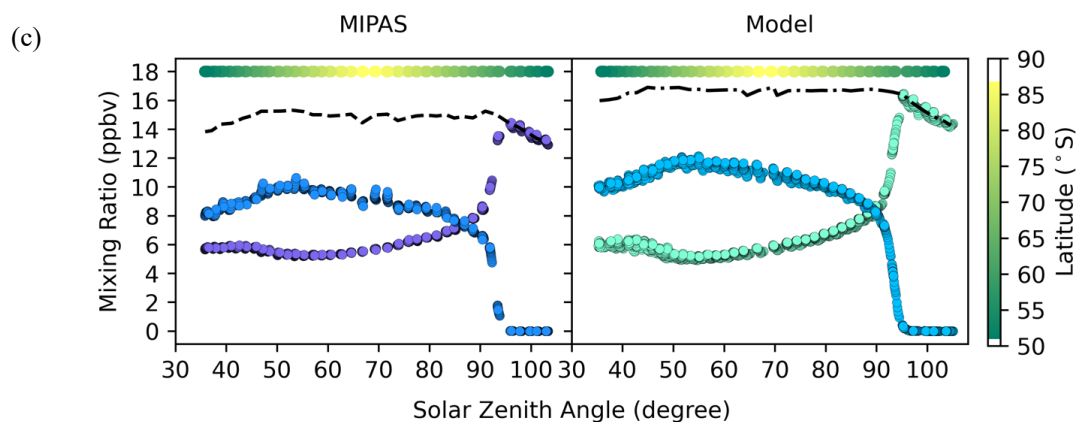
113 To better understand the diurnal variation of NO_x , concentrations of NO and NO_2 from MIPAS and the model are shown in Fig.
 114 2 at different altitudes. The NO and NO_2 concentrations from MIPAS and the model show very good overall consistency. The
 115 solar zenith angle of 90 degrees is a clear dividing line, showing that light drives the diurnal variation, and the results are in good
 116 accord with the theory.



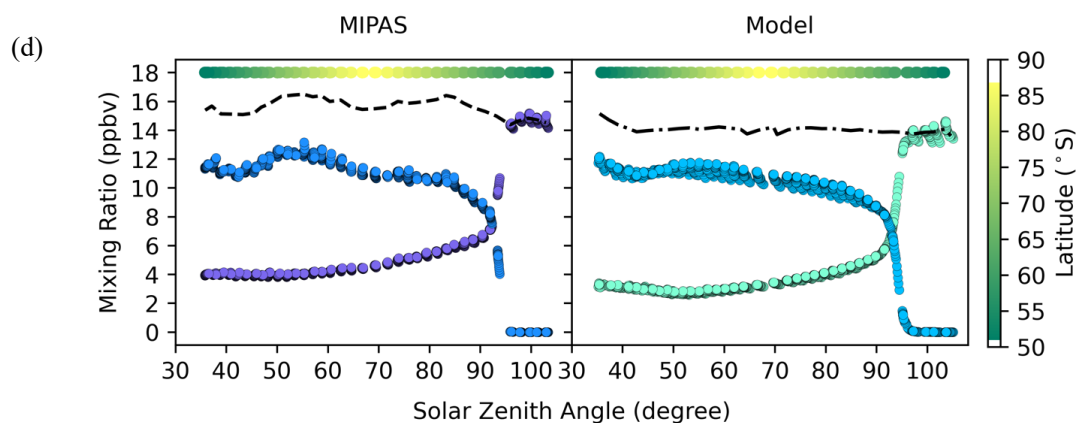
117



118



119



120

121 Figure 2. The concentrations of NO, NO₂ and NO_x in 50° S-90° S in December 2009 from MIPAS and the model at different
122 altitudes. (a) 23 km (b) 28 km (c) 33 km (d) 38km. Model values are at the same time and location as the satellite data. The color
123 bar represents the latitude of the data points at each solar zenith angle. Each point represents the four-day running mean of the
124 average concentration of multiple daily measurements at two latitude degree intervals.

125

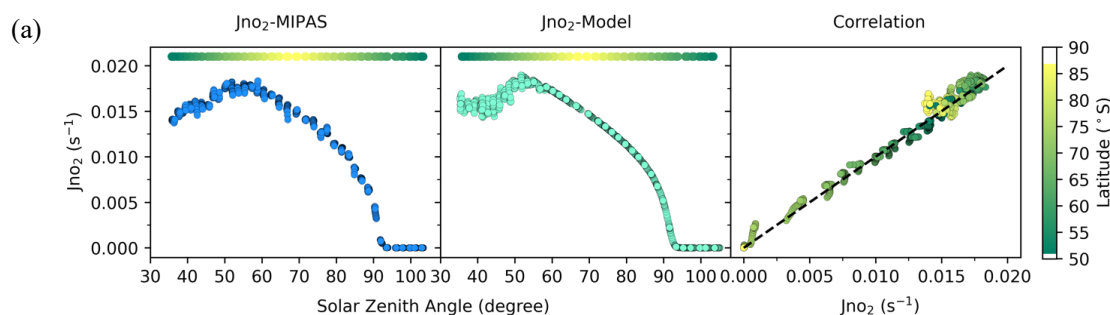
126



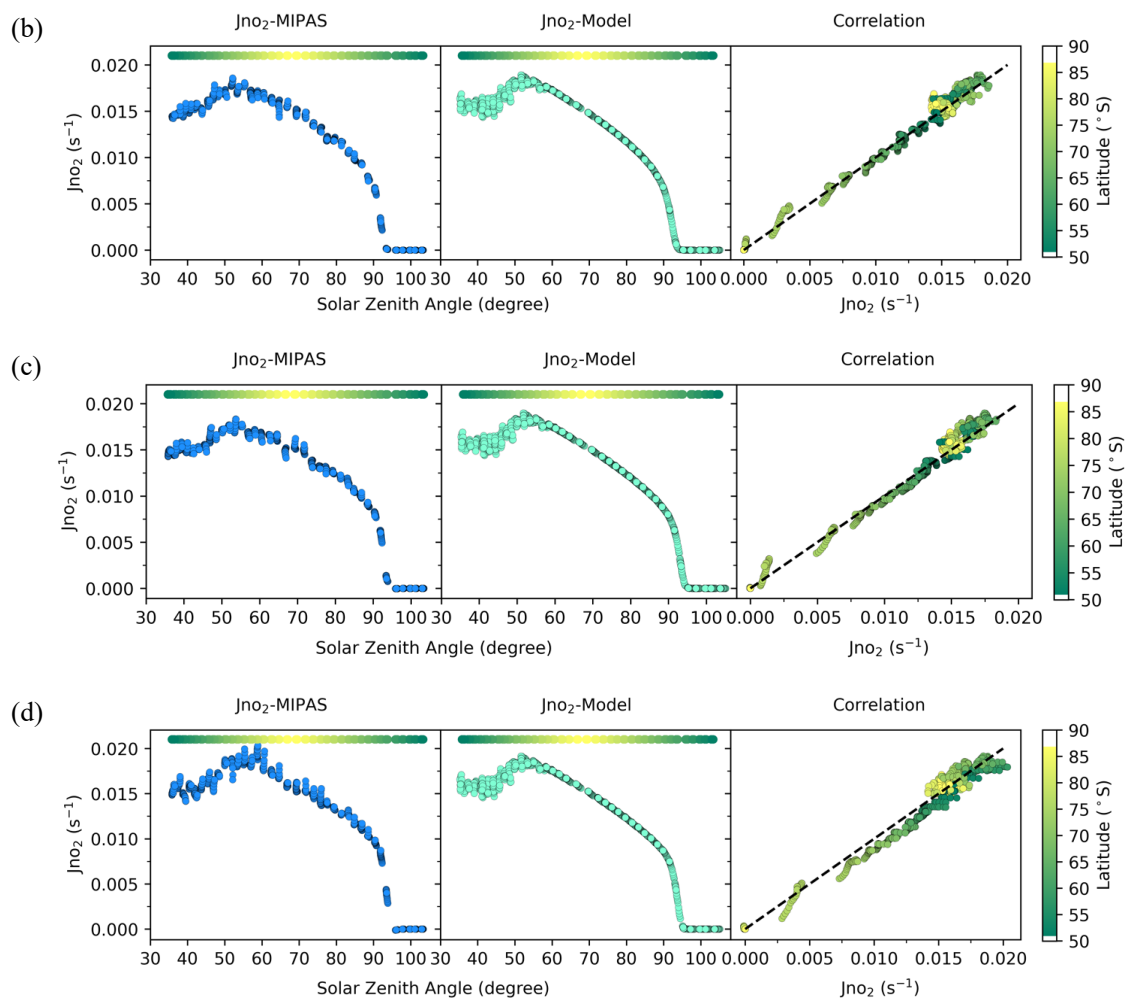
127 NO and NO₂ exchange with one another but their sum (NO_x) varies relatively little for solar zenith angles less than about 90°. An
 128 increase in NO is matched by a decrease in NO₂ for zenith angles from about 30-50°, and then decreases at larger angles, mainly
 129 reflecting changes in the photolysis rate as the satellite sweeps across the mid-latitudes and polar cap (see below). NO rapidly
 130 disappears when the solar zenith angle exceeds 90 degrees, so the concentrations of NO and NO₂ change dramatically during
 131 twilight. NO decreases rapidly and NO₂ increases rapidly. When the solar zenith angle is more than 90 degrees at these altitudes,
 132 NO is completely oxidized to NO₂, so there is no NO and NO₂/NO_x is 1. In addition, the concentration of NO₂ decreases when the
 133 solar zenith angle is more than 90 degrees, which indicates the formation of the N₂O₅.
 134 It should also be noted that in Fig. 2, the concentrations of NO and NO₂ also reflect latitude variations, because the data at each
 135 zenith angle come from different latitudes as shown by the color bar at the top of each panel in Fig. 2, but these variations are fairly
 136 small over the summer polar cap and consistent with the model as shown. From 23 km to 33 km, the concentrations of NO and
 137 NO₂ increase with the altitude.

138 3.2 J_{NO₂} at different altitudes and solar zenith angles

139 Using Eq. (2) above, the J_{NO₂} at different altitudes is shown in Fig. 3 along with the calculated J_{NO₂} values from the model. The
 140 correlation diagrams show that the values inferred from the satellite observations are in excellent agreement with the model. Fig.
 141 3 shows that from 20-40 km, the J_{NO₂} values at different altitudes are nearly the same. This indicates the weak dependence of J_{NO₂}
 142 value on altitude, which was also reported by Madronich et al. (1985). This is because the NO₂ photolysis is largely driven by
 143 wavelengths ranging from 300 nm to 420nm (Madronich et al., 1983). This spectral region is relatively free of atmospheric
 144 absorption, so the flux is nearly the same at different altitudes. When the solar zenith angle is higher than about 90 degrees, the
 145 J_{NO₂} value drops rapidly to 0. To illustrate how different species affect our calculations at some altitudes, the effects of different
 146 gases at 38 km are shown in Fig. S1. The figure shows that O₃, O and ClO are critical to NO_x chemistry at 38 km. However, the
 147 concentrations of ClO and O are smaller at altitudes of less than 35 km, and have about 3.6% and less than 12% influence in our
 148 calculations, respectively. Moreover, the satellite data error of ClO becomes large at lower levels, so ClO is not considered here
 149 when the altitude is lower than 35km.
 150



151



152

153

154

155 Figure 3. The J_{NO₂} in 50° S-90° S from MIPAS and the model at different altitudes. (a) 23 km (b) 28 km (c) 33 km (d) 38km.

156 Model values are for the same time and location as the satellite data. The color bar represents the latitude of the data points at
 157 nearly the same solar zenith angle. Each point in J_{NO₂}-Model and J_{NO₂}-MIPAS represents the four-day running mean of the average
 158 J_{NO₂} of multiple daily measurements at two latitude degree intervals. In the correlation plots, the abscissa is J_{NO₂}-MIPAS and the
 159 ordinate is the J_{NO₂}-Model and the slope of dashed line is 1.

160 3.3 J_{NO₂} at different latitudes

161 The J_{NO₂} values from the satellite and model at different latitudes are next discussed. The clear relationship between J_{NO₂} and
 162 latitude from MIPAS and model is also displayed in Fig. 4, and the close comparison between the two is remarkable. It is obvious
 163 that the satellite-inferred J_{NO₂} monotonically increases with latitude from 30° S-70° S, and then decreases at higher latitudes. The
 164 J_{NO₂} over the pole is taken at a larger solar zenith angle, which explains its decrease relative to surrounding parts of Antarctica.
 165 Fig. 5 displays maps of the detailed distributions of J_{NO₂} from MIPAS and model, which exhibits their excellent consistency and
 166 shows a sharp transition between mid-latitudes and the Antarctic continent or regions covered by sea ice.

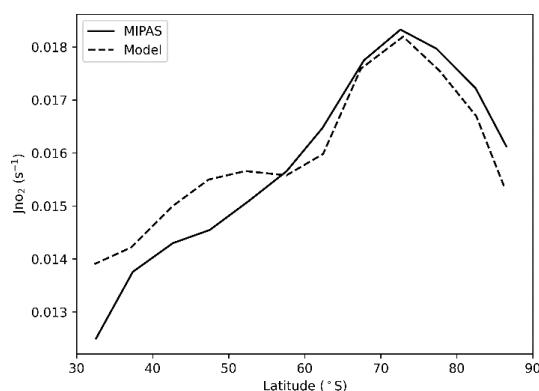


167 The sharp transitions in J_{NO_2} values shown in Fig. 5 can only be caused by the large difference in albedo between the ocean and
 168 the Antarctic environs, covered by sea ice, land ice, and snow (Brandt et al., 2005; Shao and Ke, 2015). Albedo has a strong
 169 influence on J_{NO_2} because NO_2 is more sensitive than most atmospheric species to the effects of scattering and reflection
 170 (Madronich et al., 1983; Madronich, 1987; Bösch et al., 2001; Laepple et al., 2005). In the high latitude area, the ground is covered
 171 with ice and snow, and the albedo can be as high as 0.9, while in the lower latitudes, the albedo is about 0.1 (Brandt et al., 2005;
 172 Shao and Ke, 2015). Table 1 shows the J_{NO_2} values at different solar zenith angles under different albedos. The results show that
 173 the albedo has a strong influence on the values, especially at low solar zenith angles. Based on Fig. 5, the J_{NO_2} above the continental
 174 ice is greater than that above the Antarctic sea ice, which may be because the fraction of open water within the pack influences the
 175 albedo (Brandt et al., 2005).

176

177

178

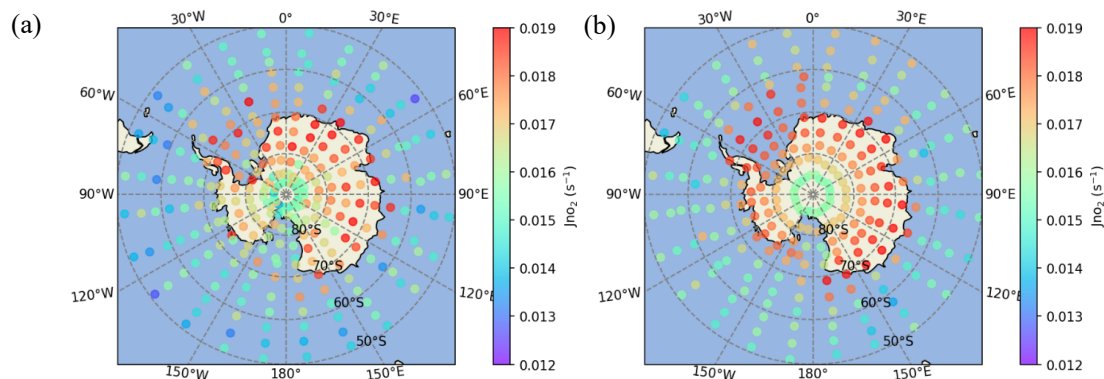


179

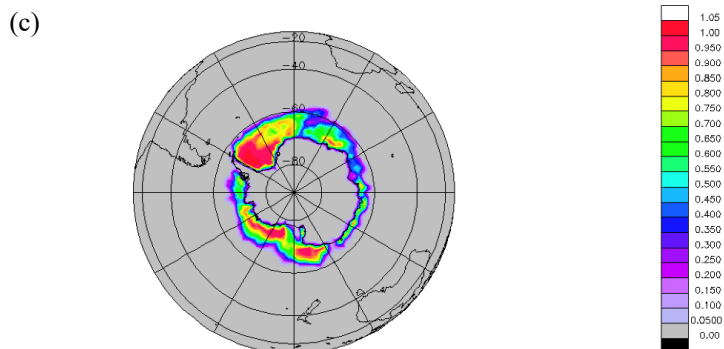
180 Figure 4. The relationship between J_{NO_2} and latitude from MIPAS and model in 30° S-90° S at 28 km. Model data are for the

181 same time and location as the satellite data. J_{NO_2} is examined wherever the solar zenith angle is less than 70 degrees and

182 averaged every five degrees of latitude.



183



184

185 Figure 5. The mapping of J_{NO_2} in 50°S - 90°S at 28 km from (a) MIPAS and (b) model. (c) The distribution of the sea ice extent
 186 in December, 2009 in Antarctica and its albedo, from the model. Model J_{NO_2} data are for the same time and location as the
 187 satellite data. J_{NO_2} is shown wherever the solar zenith angle is less than 70 degrees and averaged every 3.33° latitude \times 15°
 188 longitude.

189

190

Table 1. J_{NO_2} at different solar zenith angles under different albedos (α)

Solar zenith angle	J_{NO_2} ($\alpha = 0.1$)	J_{NO_2} ($\alpha = 0.9$)	J_{NO_2} ($\alpha = 0.9$)/ J_{NO_2} ($\alpha = 0.1$)
0	1.30	2.21	1.70
10	1.30	2.19	1.69
20	1.29	2.14	1.65
30	1.28	2.05	1.59
40	1.27	1.92	1.52
50	1.24	1.77	1.42
60	1.20	1.58	1.31
70	1.14	1.36	1.20
80	1.01	1.10	1.09
90	0.664	0.673	1.01

191

192 4 Conclusions

193 The diurnal variations of NO_x species and the resulting J_{NO_2} from about 50°S - 90°S in December in 20-40 km have been evaluated
 194 based on MIPAS data. Light has a strong impact on the diurnal variations. NO and NO₂ are in steady state in the daytime and their
 195 sum is almost constant.



196 The calculated J_{NO_2} remarkably consistent with the model results, and the J_{NO_2} value decreases as the solar zenith angle increases.
197 The J_{NO_2} value drops rapidly to 0 at the solar zenith angle of about 90 degrees. Moreover, the weak dependence of the J_{NO_2} value
198 on altitude in this region is evident.

199 The results from the satellite and the model both indicate that J_{NO_2} increases with latitude, which can be attributed to more reflected
200 light from ice and snow surfaces with high albedo. In summary, this work presents a new method for obtaining accurate J_{NO_2}
201 values based on satellite data. Further, this method can be extended to other photodissociation coefficients, paving the way for
202 further tests of global photodissociation coefficients data based on satellites.

203

204 **Code and data availability.** The data and code are available at <https://doi.org/10.5281/zenodo.7764756>.

205 **Supplement.**

206 **Author contributions.** S.S. designed the study. J. G. analyzed the data and produced the figures. S. M. and D. K. run the models
207 and contributed significantly to the interpretation of findings. J.G. wrote the manuscript, with comments from all authors.

208 **Competing interests.** The contact author has declared that none of the authors has any competing interests.

209 **Disclaimer.** Publisher's note: Copernicus Publications remains neutral with regard to jurisdictional claims in published maps and
210 institutional affiliations.

211 **Acknowledgements.** Doug Kinnison was funded in part by NASA (grant no. 80NSSC19K0952). SS acknowledges support as the
212 Martin Professor of environmental studies at MIT, while JG appreciates an MIT presidential fellowship. SM acknowledges partial
213 support by the US Department of Agriculture (USDA) UV-B Monitoring and Research Program, Colorado State University, under
214 USDA National Institute of Food and Agriculture Grant 2019-34263-30552; 2022-34263-38472. The CESM project is supported
215 by the National Science Foundation and the Office of Science (BER) of the U.S. Department of Energy. We gratefully acknowledge
216 high-performance computing support from Cheyenne (doi:10.5065/D6RX99HX) provided by NCAR's Computational and
217 Information Systems Laboratory, sponsored by the National Science Foundation. We thank the Institute of Meteorology and
218 Climate Research - Atmospheric Trace Gases and Remote Sensing, and Dr. Michael Kiefer and Dr. Gabriele Stiller for MIPAS
219 data.

220

221 References

- 222 Anderson, G., Gille, J., Bailey, P., and Solomon, S.: LRIR observations of diurnal ozone variation in the mesosphere,
223 Quadrennial International Ozone Symposium, 580–585, 1981.
- 224 Bösch, H., Camy-Peyret, C., Chipperfield, M., Fitzenberger, R., Harder, H., Schiller, C., Schneider, M., Trautmann, T.,
225 and Pfeilsticker, K.: Comparison of measured and modeled stratospheric UV/Visible actinic fluxes at large solar
226 zenith angles, *Geophys. Res. Lett.*, 28, 1179–1182, <https://doi.org/10.1029/2000GL012134>, 2001.
- 227 Brandt, R. E., Warren, S. G., Worby, A. P., and Grenfell, T. C.: Surface Albedo of the Antarctic Sea Ice Zone, *J. Climate*,
228 18, 3606–3622, <https://doi.org/10.1175/JCLI3489.1>, 2005.
- 229 Burkholder, J. B., Sander, S. P., Abbatt, J. P. D., Barker, J. R., Huie, R. E., Kolb, C. E., Kurylo, M. J., Orkin, V. L.,
230 Wilmouth, D. M., and Wine, P. H.: Chemical kinetics and photochemical data for use in atmospheric studies:



- 231 evaluation number 18, Pasadena, CA: Jet Propulsion Laboratory, National Aeronautics and Space
232 Administration, 2015.
- 233 Crutzen, P. J.: The influence of nitrogen oxides on the atmospheric ozone content, *Quarterly Journal of the Royal*
234 *Meteorological Society*, 96, 320–325, <https://doi.org/10.1002/qj.49709640815>, 1970.
- 235 Crutzen, P. J.: The Role of NO and NO₂ in the Chemistry of the Troposphere and Stratosphere, *Annu. Rev. Earth Planet.*
236 *Sci.*, 7, 443–472, <https://doi.org/10.1146/annurev.ea.07.050179.002303>, 1979.
- 237 Danabasoglu, G., Lamarque, J. -F., Bacmeister, J., Bailey, D. A., DuVivier, A. K., Edwards, J., Emmons, L. K., Fasullo,
238 J., Garcia, R., Gettelman, A., Hannay, C., Holland, M. M., Large, W. G., Lauritzen, P. H., Lawrence, D. M.,
239 Lenaerts, J. T. M., Lindsay, K., Lipscomb, W. H., Mills, M. J., Neale, R., Oleson, K. W., Otto-Bliesner, B.,
240 Phillips, A. S., Sacks, W., Tilmes, S., Kampenhout, L., Vertenstein, M., Bertini, A., Dennis, J., Deser, C.,
241 Fischer, C., Fox-Kemper, B., Kay, J. E., Kinnison, D., Kushner, P. J., Larson, V. E., Long, M. C., Mickelson,
242 S., Moore, J. K., Nienhouse, E., Polvani, L., Rasch, P. J., and Strand, W. G.: The Community Earth System
243 Model Version 2 (CESM2), *J. Adv. Model. Earth Syst.*, 12, <https://doi.org/10.1029/2019MS001916>, 2020.
- 244 Del Negro, L. A., Fahey, D. W., Gao, R. S., Donnelly, S. G., Keim, E. R., Neuman, J. A., Cohen, R. C., Perkins, K. K.,
245 Koch, L. C., Salawitch, R. J., Lloyd, S. A., Proffitt, M. H., Margitan, J. J., Stimpfle, R. M., Bonne, G. P., Voss,
246 P. B., Wennberg, P. O., McElroy, C. T., Swartz, W. H., Kusterer, T. L., Anderson, D. E., Lait, L. R., and Bui,
247 T. P.: Comparison of modeled and observed values of NO₂ and JNO₂ during the Photochemistry of Ozone Loss
248 in the Arctic Region in Summer (POLARIS) mission, *J. Geophys. Res.*, 104, 26687–26703,
249 <https://doi.org/10.1029/1999JD900246>, 1999.
- 250 Fabian, P., Pyle, J. A., and Wells, R. J.: Diurnal variations of minor constituents in the stratosphere modeled as a function
251 of latitude and season, *J. Geophys. Res.*, 87, 4981, <https://doi.org/10.1029/JC087iC07p04981>, 1982.
- 252 Fischer, H., Birk, M., Blom, C., Carli, B., Carlotti, M., Endemann, M., Flaud, J. M., Gessner, R., Kleinert, A., Koopman,
253 R., Langen, J., Lopez-Puertas, M., Mosner, P., Nett, H., Oelhaf, H., Perron, G., Remedios, J., Ridolfi, M., Stiller,
254 G., and Zander, R.: MIPAS: an instrument for atmospheric and climate research, *Atmos. Chem. Phys.*,
255 <https://doi.org/10.5194/acp-8-2151-2008>, 2008.
- 256 Funke, B., García-Comas, M., Glatthor, N., Grabowski, U., Kellmann, S., Kiefer, M., Linden, A., López-Puertas, M., Stiller,
257 G. P., and von Clarmann, T.: MIPAS IMK/IAA version 8 retrieval of nitric oxide and lower thermospheric
258 temperature, *Atmos. Meas. Tech. Discuss.* [preprint], <https://doi.org/10.5194/amt-2022-260>, in review, 2022.
- 259 Gelaro, R., McCarty, W., Suárez, M. J., Todling, R., Molod, A., Takacs, L., Randles, C. A., Darmenov, A., Bosilovich, M.
260 G., Reichle, R., Wargan, K., Coy, L., Cullather, R., Draper, C., Akella, S., Buchard, V., Conaty, A., da Silva,
261 A. M., Gu, W., Kim, G.-K., Koster, R., Lucchesi, R., Merkova, D., Nielsen, J. E., Partyka, G., Pawson, S.,
262 Putman, W., Rienecker, M., Schubert, S. D., Sienkiewicz, M., and Zhao, B.: The Modern-Era Retrospective
263 Analysis for Research and Applications, Version 2 (MERRA-2), *J. Climate*, 30, 5419–5454,
264 <https://doi.org/10.1175/JCLI-D-16-0758.1>, 2017.
- 265 Gettelman, A., Mills, M. J., Kinnison, D. E., Garcia, R. R., Smith, A. K., Marsh, D. R., Tilmes, S., Vitt, F., Bardeen, C. G.,
266 McInerney, J., Liu, H. -L., Solomon, S. C., Polvani, L. M., Emmons, L. K., Lamarque, J. -F., Richter, J. H.,
267 Glanville, A. S., Bacmeister, J. T., Phillips, A. S., Neale, R. B., Simpson, I. R., DuVivier, A. K., Hodzic, A.,
268 and Randel, W. J.: The Whole Atmosphere Community Climate Model Version 6 (WACCM6), *JGR*
269 *Atmospheres*, 124, 12380–12403, <https://doi.org/10.1029/2019JD030943>, 2019.



- 270 Johnston, H.: Reduction of Stratospheric Ozone by Nitrogen Oxide Catalysts from Supersonic Transport Exhaust, *Science*,
271 173, 517–522, <https://doi.org/10.1126/science.173.3996.517>, 1971.
- 272 Junkermann, W., Platt, U., and Volz-Thomas, A.: A photoelectric detector for the measurement of photolysis frequencies
273 of ozone and other atmospheric molecules, *J. Atmos. Chem.*, 8, 203–227, <https://doi.org/10.1007/BF00051494>,
274 1989.
- 275 Kawa, S. R., Fahey, D. W., Solomon, S., Brune, W. H., Proffitt, M. H., Toohey, D. W., Anderson, D. E., Anderson, L. C.,
276 and Chan, K. R.: Interpretation of aircraft measurements of NO, ClO, and O₃ in the lower stratosphere, *J.*
277 *Geophys. Res.*, 95, 18597, <https://doi.org/10.1029/JD095iD11p18597>, 1990.
- 278 Kiefer, M., von Clarmann, T., Funke, B., García-Comas, M., Glatthor, N., Grabowski, U., Kellmann, S., Kleinert, A.,
279 Laeng, A., Linden, A., López-Puertas, M., Marsh, D. R., and Stiller, G. P.: IMK/IAA MIPAS temperature
280 retrieval version 8: nominal measurements, *Atmos. Meas. Tech.*, 14, 4111–4138, [https://doi.org/10.5194/amt-](https://doi.org/10.5194/amt-14-4111-2021)
281 [14-4111-2021](https://doi.org/10.5194/amt-14-4111-2021), 2021.
- 282 Kiefer, M., von Clarmann, T., Funke, B., Garcia-Comas, M., Glatthor, N., Grabowski, U., Höpfner, M., Kellmann, S.,
283 Laeng, A., Linden, A., Lopez-Puertas, M., and Stiller, G.: Version 8 IMK/IAA MIPAS ozone profiles: nominal
284 observation mode, *Atmos. Meas. Tech.*, 16, 1443–1460, <https://doi.org/10.5194/amt-16-1443-2023>, 2023.
- 285 Kinnison, D. E., Brasseur, G. P., Walters, S., Garcia, R. R., Marsh, D. R., Sassi, F., Harvey, V. L., Randall, C. E., Emmons,
286 L., Lamarque, J. F., Hess, P., Orlando, J. J., Tie, X. X., Randel, W., Pan, L. L., Gettelman, A., Granier, C.,
287 Diehl, T., Niemeier, U., and Simmons, A. J.: Sensitivity of chemical tracers to meteorological parameters in the
288 MOZART-3 chemical transport model, *J. Geophys. Res.*, 112, D20302, <https://doi.org/10.1029/2006JD007879>,
289 2007.
- 290 Laeng, A., Hubert, D., Verhoelst, T., von Clarmann, T., Dinelli, B. M., Dudhia, A., Raspollini, P., Stiller, G., Grabowski,
291 U., Keppens, A., Kiefer, M., Sofieva, V., Froidevaux, L., Walker, K. A., Lambert, J.-C., and Zehner, C.: The
292 ozone climate change initiative: Comparison of four Level-2 processors for the Michelson Interferometer for
293 Passive Atmospheric Sounding (MIPAS), *Remote Sensing of Environment*, 162, 316–343,
294 <https://doi.org/10.1016/j.rse.2014.12.013>, 2015.
- 295 Laepple, T., Schultz, M. G., Lamarque, J. F., Madronich, S., Shetter, R. E., Lefer, B. L., and Atlas, E.: Improved albedo
296 formulation for chemistry transport models based on satellite observations and assimilated snow data and its
297 impact on tropospheric photochemistry, *J. Geophys. Res.*, 110, D11308, <https://doi.org/10.1029/2004JD005463>,
298 2005.
- 299 Madronich, S.: Photodissociation in the atmosphere: 1. Actinic flux and the effects of ground reflections and clouds, *J.*
300 *Geophys. Res.*, 92, 9740, <https://doi.org/10.1029/JD092iD08p09740>, 1987.
- 301 Madronich, S. and Weller, G.: Numerical integration errors in calculated tropospheric photodissociation rate coefficients,
302 *J. Atmos. Chem*, 10, 289–300, <https://doi.org/10.1007/BF00053864>, 1990.
- 303 Madronich, S., Hastie, D. R., Ridley, B. A., and Schiff, H. I.: Measurement of the photodissociation coefficient of NO₂ in
304 the atmosphere: I. Method and surface measurements, *J. Atmos. Chem.*, 1, 3–25,
305 <https://doi.org/10.1007/BF00113977>, 1983.
- 306 Madronich, S., Hastie, D. R., Schiff, H. I., and Ridley, B. A.: Measurement of the photodissociation coefficient of NO₂ in
307 the atmosphere: II, stratospheric measurements, *J. Atmos. Chem.*, 3, 233–245,
308 <https://doi.org/10.1007/BF00210498>, 1985.



- 309 Pommereau, J. P.: Observation of NO₂ diurnal variation in the stratosphere, *Geophys. Res. Lett.*, 9, 850–853,
310 <https://doi.org/10.1029/GL009i008p00850>, 1982.
- 311 Roscoe, H. K., Kerridge, B. J., Gray, L. J., Wells, R. J., and Pyle, J. A.: Simultaneous measurements of stratospheric NO
312 and NO₂ and their comparison with model predictions, *J. Geophys. Res.*, 91, 5405,
313 <https://doi.org/10.1029/JD091iD05p05405>, 1986.
- 314 Shao, Z.-D. and Ke, C.-Q.: Spring–summer albedo variations of Antarctic sea ice from 1982 to 2009, *Environ. Res. Lett.*,
315 10, 064001, <https://doi.org/10.1088/1748-9326/10/6/064001>, 2015.
- 316 Sheese, P. E., Walker, K. A., Boone, C. D., McLinden, C. A., Bernath, P. F., Bourassa, A. E., Burrows, J. P., Degenstein,
317 D. A., Funke, B., Fussen, D., Manney, G. L., McElroy, C. T., Murtagh, D., Randall, C. E., Raspollini, P.,
318 Rozanov, A., Russell III, J. M., Suzuki, M., Shiotani, M., Urban, J., von Clarmann, T., and Zawodny, J. M.:
319 Validation of ACE-FTS version 3.5 NO_y species profiles using correlative satellite measurements, *Atmos.*
320 *Meas. Tech.*, 9, 5781–5810, <https://doi.org/10.5194/amt-9-5781-2016>, 2016.
- 321 Shetter, R. E., McDaniel, A. H., Cantrell, C. A., Madronich, S., and Calvert, J. G.: Actinometer and Eppley radiometer
322 measurements of the NO₂ photolysis rate coefficient during the Mauna Loa Observatory photochemistry
323 experiment, *J. Geophys. Res.*, 97, 10349, <https://doi.org/10.1029/91JD02289>, 1992.
- 324 Solomon, S., Russell, J. M., and Gordley, L. L.: Observations of the diurnal variation of nitrogen dioxide in the stratosphere,
325 *J. Geophys. Res.*, 91, 5455, <https://doi.org/10.1029/JD091iD05p05455>, 1986.
- 326 Von Clarmann, T., Höpfner, M., Kellmann, S., Linden, A., Chauhan, S., Funke, B., Grabowski, U., Glatthor, N., Kiefer,
327 M., and Schiederdecker, T.: Retrieval of temperature, H₂O, O₃, HNO₃, CH₄, N₂O, ClONO₂ and ClO from
328 MIPAS reduced resolution nominal mode limb emission measurements, *Atmos. Meas. Tech.*, 2, 159–175,
329 <https://doi.org/10.5194/amt-2-159-2009>, 2009.
- 330 Webster, C. R. and May, R. D.: Simultaneous in situ measurements and diurnal variations of NO, NO₂, O₃, *j*NO₂, CH₄,
331 H₂O, and CO₂ in the 40- to 26-km region using an open path tunable diode laser spectrometer, *J. Geophys. Res.*,
332 92, 11931, <https://doi.org/10.1029/JD092iD10p11931>, 1987.
- 333 Wetzel, G., Bracher, A., Funke, B., Goutail, F., Hendrick, F., Bazureau, A., Belotti, C., Blumenstock, T., Maziere, M. D.,
334 Fischer, H., Huret, N., Ionov, D., Lopez-Puertas, M., Maucher, G., Oelhaf, H., and Zhang, G.: Validation of
335 MIPAS-ENVISAT NO₂ operational data, *Atmos. Chem. Phys.*, 2007.
- 336